Supporting Information

Multi-Doping of Si Cages: High Spin States beyond the Single-Dopant Septet Limit

Dennis Palagin, Tobias Teufl and Karsten Reuter

Department Chemie, Technische Universität München, Lichtenbergstr. 4, D-85747 Garching, Germany

1. Computational details

All calculations have been performed with the all-electron full-potential density-functional theory (DFT) code FHI-aims [1-2]. Electronic exchange and correlation was treated within the hybrid functional level using the PBE0 [3] functional. All sampling calculations are done with the "tier1" basis set. The numerical integrations have been performed with the "tight" settings, which correspond to e.g. integration grids with 85 and 101 radial shells for Si and Cr, respectively, in which the number of integration points is successively decreased from 434 for the outermost shell to 50 for the innermost one. For the ensuing electronic structure analysis of the optimized geometries the electron density was recomputed with an enlarged "tier3" basis set, which contains 64 basis functions for Si and 124 basis functions for Cr. Systematic convergence tests indicate that these settings are fully converged with respect to the target quantities, such as energetic difference of different isomers in the sampling runs; electron and spin density distribution in the electronic structure analysis.

Local structure optimization is done using the Broyden-Fletcher-Goldfarb-Shanno method [4] relaxing all force components to smaller than 10^{-2} eV/Å. To make sure that we are discussing the true ground-state structure we relied on basin-hopping (BH) based global geometry optimization [5-7]. Within the BH idea the configuration space is explored by performing consecutive jumps from one local minimum of the potential energy surface (PES) to another. To achieve this, positions of atoms in the cluster are randomly perturbed in a so-called trial move followed by a local geometry optimization which brings the system again into a local PES minimum. A Metropolis-type [8] acceptance rule is used to either accept or reject the jump into the PES minimum reached by the trial move. As specific BH implementation we chose collective trial moves, in which all atoms are displaced in a random direction. Three different chemical-intuition-governed starting points were used for all optimization runs. Typical BH runs comprised of the order of 100 accepted trial moves, and unanimously identified the lowest energy structure regardless of the specific settings and starting configuration employed.

2. Geometries and electronic structure analysis of the M_2Si_{18} and $M_2Si_{18}H_{12}$ clusters

The starting point of our investigation is an extended configurational search, which confirmed that the ground-state structure of $Cr_2Si_{18}^+$ is indeed a highly symmetrical (D_{6h}) double prism (see Fig. 1b), as suggested by Kumar and Kawazoe [9] and Ji and Luo [10].

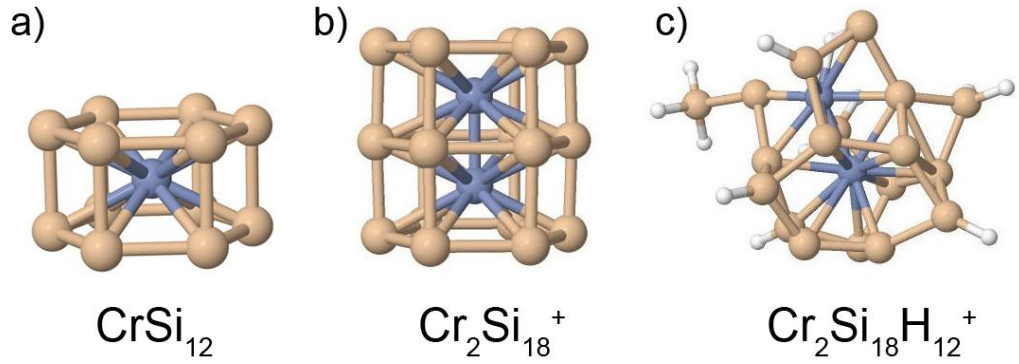

Fig. 1. *The found ground-state structures of (a) $CrSi_{12}$ (singlet), (b) $Cr_2Si_{18}^+$ and (c) $Cr_2Si_{18}H_{12}^+$ (doublets).*

An energetic difference to the next isomer of 0.68 eV and a HOMO-LUMO gap of 1.17 eV indicate a rather high stability of the symmetrical $Cr_2Si_{18}^+$ structure. As can be clearly seen from Fig. 1, the $Cr_2Si_{18}^+$ structure is basically composed of two $CrSi_{12}$ prisms [11-12] merged together. Although such a combination does not provide the possibility of achieving electronic shell closure (18×4 e^- from Si atoms + 6×2 e^- from Cr atoms – 1 e^- = 83 e^-, with the 2*d* or 1*h* shell closure requiring 68 and 90 electrons, respectively) [13-15], it does effectively saturate all Si dangling bonds through the strong Cr-Si interaction, thus stabilizing the identified geometrical structure.

To check if the hydrogen termination idea [16-20] is applicable in our case, we also run a global geometry optimization of the hydrogen-terminated $Cr_2Si_{18}H_{12}^+$ structure. The found ground-state structure has a heavily distorted geometry, presented in the Fig. 1c. In contrast to previous results reported by Kumar and Kawazoe [18] (based on local optimization), the symmetric hydrogenated double-prism is only a local minimum, lying 1.81 eV higher than the here identified ground-state structure. This may be explained by the strong interaction between Si and H atoms, trying to saturate Si dangling bonds. With the apparently insufficient space within the cluster to keep the dopant atoms inside, the structure ends up with a complex combination of Si-H and Si-Cr interactions which makes the double prism geometry unstable and leads to the "explosion" of the structure. This result agrees well with previously reported insufficient space within $Si_{16}H_{16}$ clusters for conserving any 3*d* metal dopants [17]. While in case of $Si_{16}H_{16}$ the average radius of the cage is about 3Å, here in the symmetric $Cr_2Si_{18}^+$ cluster the dopant-cage

distance amounts only to 2.67Å, which makes the concept of conservation of the atomic character of the magnetic dopant impossible. Similar results were obtained for other dopant species like Fe.

Therefore, it is evident that the Si_{18} cluster is generally too small to accommodate two dopants with their magnetic character preserved. Thus, we need to take a look at larger Si_nH_n cages in order to be able to stabilize multiple magnetic dopants. As we have reported earlier [17], extensive sampling runs suggest empty cage geometries as ground states for the larger hydrogenated Si fullerenes, such as $Si_{20}H_{20}$, $Si_{24}H_{24}$, $Si_{26}H_{26}$ and $Si_{28}H_{28}$. Eventually, these cages should offer enough space to also host multicore dopants, which might allow achieving higher magnetic moments than those available through encapsulation of single-atom transition metals.

3. Cr_2, Cr_2^+, Mn_2, Mn_2^+ and $CrMn^+$ dimer dopants

T. Lau *et al.* have reported experimental evidence for the localized character of the valence electrons in Cr_2^+, Mn_2^+ and $CrMn^+$ dimer cations [21]. With bonding predominantly mediated by 4*s* electrons, these transition-metal dimers exhibit local high spin states with up to 5 μ_B spin moment of the 3*d* electrons at each ionic core. If such dopants can preserve their unique properties when encapsulated within the Si cage, it might be a way to bring these properties to cluster-assembled materials, for example by constructing doubly Si-Si bound aggregates, as we have recently suggested [16].

The first question we have to answer is whether the suggested dimers (Cr_2^+, Mn_2^+ and $CrMn^+$) are indeed highly magnetic. For this, we optimized the geometries of all three dimers for all possible spin states at the hybrid functional level using the PBE0 functional. Considering the frequent observation that hybrid functional DFT yields results for 3*d* transition metal containing systems that are at least en par, to correlated wave function approaches [22-25], this supports the reliability of the results reported here. The obtained results are then compared to the neutral Cr_2 and Mn_2 dimers in order to discuss the difference in their electronic structure.

Table 1 summarizes the obtained results for the cationic dimers. In good agreement with experiment [21], Cr_2^+ and Mn_2^+ both exhibit ground-state configurations with 11 unpaired electrons. Since the 3*d* electrons are localized at the metal cores in both clusters, bonding is predominantly mediated by the remaining 4*s* electron, shared between the two atoms (Cr_2^+), or the remaining three 4*s* electrons situated in a fully occupied bonding and a singly occupied antibonding σ-orbital (Mn_2^+). The experimentally observed values of the bond energies of about 1.4 eV [26-27] also agree well with the obtained results.

unpaired e^-	*M-M* distance, Å	Relative energy, eV	Binding energy, eV
Cr_2^+			
11	**2.90**	**0.00**	**1.55**
9	2.64	1.03	0.52
7	2.28	3.24	-1.68
5	1.77	3.74	-2.18
3	1.65	4.31	-2.76
1	1.56	4.24	-2.68
Mn_2^+			
13	4.18	2.51	-0.83
11	**2.93**	**0.00**	**1.68**
9	2.48	0.97	0.71
7	2.13	3.67	-1.99
5	1.90	5.43	-3.75
3	1.73	7.46	-5.78
1	1.63	7.14	-5.46
$CrMn^+$			
12	3.34	0.90	0.61
10	**2.80**	**0.00**	**1.51**
8	2.44	1.72	-0.22
6	2.29	4.40	-2.89
4	1.81	4.45	-2.95
2	1.60	5.54	-4.04
0	1.61	6.07	-4.56

Table 1. *Optimized M-M distances, relative stabilities and binding energies (all calculated using PBE0 functional with tier3 basis set) for all possible spin states of Cr_2^+, Mn_2^+ and $CrMn^+$ dimers.*

In $CrMn^+$, two 4*s* orbitals occupy a bonding orbital, leading to the overall number of ten unpaired 3*d* electrons. In all cases the rather high bond lengths (2.80 to 2.93 Å) confirm that only *s*-electrons contribute to bonding. Despite of being isoelectronic to the neutral Cr_2 dimer, $CrMn^+$ shows a very different electronic structure. Cr_2 is a singlet with a formal sextuple bond, exhibiting a bond length of only 1.59 Å, which agrees well with the experimental value of 1.68 Å [28]. Mn_2, on the other hand, is an only weakly bound (0.17 eV) dimer with a very long equilibrium distance of 3.48 Å (Table 2), and can be described as a van der Waals molecule.

Again, this agrees perfectly with the experimentally reported values of the bond length (3.4 Å) and the bond energy (0.44±0.30 eV), cf. ref. [29-30].

unpaired e^-	*M-M* distance, Å	Relative energy, eV	Binding energy, eV
Cr_2			
12	3.23	1.36	0.11
10	2.71	0.98	0.49
8	2.38	2.56	-1.08
6	2.04	2.40	-0.93
4	1.79	1.47	0.00
2	1.68	1.02	0.45
0	**1.59**	**0.00**	**1.47**
Mn_2			
14	2.88	3.49	-3.32
12	2.91	0.94	-0.78
10	**3.48**	**0.00**	**0.17**
8	2.54	1.96	-1.80
6	1.96	3.50	-3.34
4	2.21	5.23	-5.06
2	2.49	8.36	-8.19
0	1.64	5.61	-5.44

Table 2. *Optimized M-M distances, relative stabilities and binding energies (all calculated using PBE0 functional with tier3 basis set) for all possible spin states of Cr_2 and Mn_2 dimers.*

Thus, a strong 3*d* valence electron localization in Cr_2^+, Mn_2^+ and $CrMn^+$ dimers due to the half-filled 3*d* shells of Cr and Mn atoms, observed in the core-level X-ray absorption spectroscopy experiments [22], is also confirmed by DFT calculations at the hybrid PBE0 functional level.

4. Detailed analysis of the identified geometries and stabilization mechanisms within $M_2^+@Si_{24}H_{24}$ cluster aggregates

The unbiased configurational sampling reveals that the ground-state structures correspond to the highly symmetrical D_{6d} structure (Fig. 2a) with 11 unpaired electrons (structure I). Interestingly, this turned out to be not the only possible structure with a Cr_2^+ dimer encapsulated within the cage. Fig. 2b illustrates another high-spin isomer with the dimer oriented perpendicular

to the cage's principal axis, which corresponds to the C_{2v} symmetry group (structure II). This structure also has 11 unpaired electrons in total. However, it is 1.20 eV higher in energy than the ground-state structure. For comparison, the most stable compact structure (with distorted non-cage geometry) is 2.09 eV less stable than the ground-state structure.

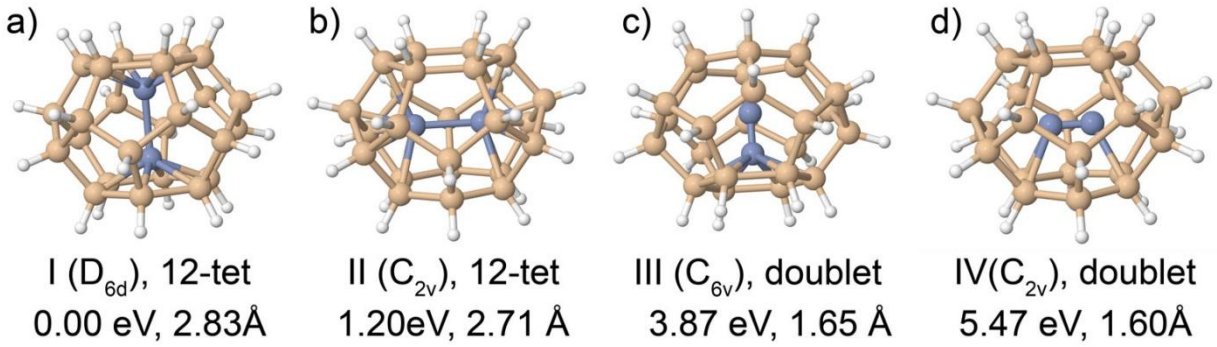

Fig. 2. *Selected cage-like structures of $Cr_2^+@Si_{24}H_{24}$ with their multiplicities, relative energies and Cr-Cr bond lengths. (a) ground-state structure (D_{6d}, structure I) with 11 unpaired electrons; (b) structure II (11 unpaired electrons, 1.20 eV above the global minimum); c) and d) – doublet structures with one unpaired electron (3.87 and 5.47 eV less stable than the ground-state structure, respectively).*

It is also possible to stabilize other spin states within the cage. For example, a doublet Cr_2^+ dimer can also be encapsulated in the $Si_{24}H_{24}$, oriented either along (structure III, C_{6v}) or perpendicular to (structure IV, C_{2v}) the cage's principal axis (see Fig. 2c and Fig. 2d). However, these structures possess much higher total energies (3.87 eV and 5.47 eV higher than the ground-state structure, respectively), which agrees well with the 4.24 eV difference between the corresponding spin states of the isolated Cr_2^+ dimer. Another peculiarity is a remarkable agreement in the bond lengths of the isolated and encapsulated Cr_2^+ dimers. In both high-spin structures the PBE0-optimized Cr-Cr bond lengths are 2.83 Å and 2.71 Å (compared to the 2.90 Å for isolated Cr_2^+ with 11 unpaired electrons), while for low-spin state structures the corresponding distances are 1.65 Å and 1.60 Å (compared to 1.56 Å in an isolated doublet Cr_2^+ dimer).

Stabilization of the high spin state of the encapsulated dimer in the $Cr_2^+@Si_{24}H_{24}$ ground-state structure, and reasonable agreement in both relative energies and equilibrium distances between the dopants encapsulated in different cage-like isomers and the isolated Cr_2^+ dimers, suggests that there should not be much interaction between the dopant dimer and the cage. On the other hand, a rather high binding energy (3.26 eV for structure I) and a notable difference between the two high-spin isomers (1.20 eV between the structure I and structure II) indicate the presence of some interaction that helps to stabilize the endohedral structure. In order to clarify

this, we plot the spin density distribution within the $Cr_2^+@Si_{24}H_{24}$ ground-state structure (see the inset in Fig. 3) and analyze the density of states (DOS) diagram (Fig. 3).

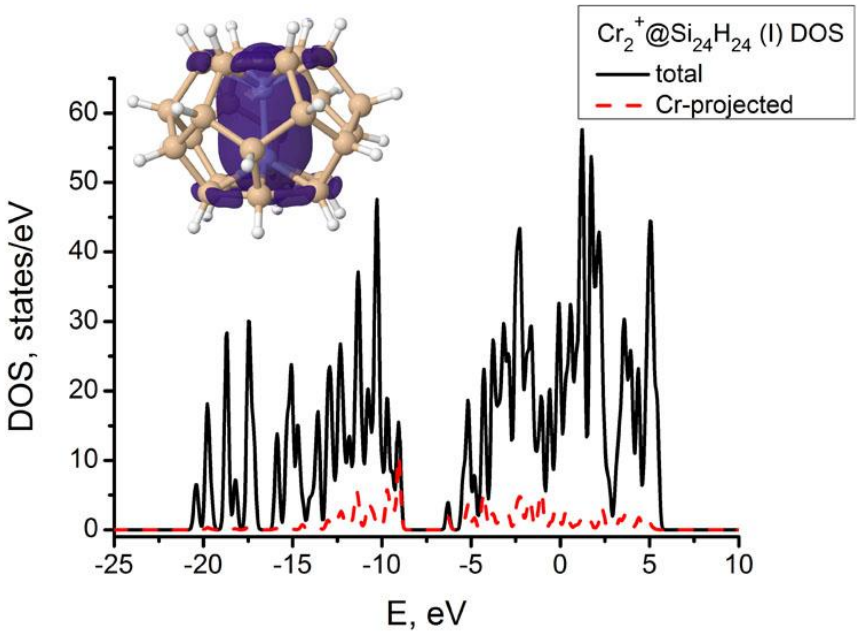

Fig. 3. *Total density of states (black solid line) and DOS projected on the metal dopant (red dashed line) for $Cr_2^+@Si_{24}H_{24}$ (structure I, ground state) calculated at the hybrid PBE0 functional level. Highest occupied state lies at -9.04 eV, lowest unoccupied state lies at -6.30 eV; vacuum level is used as reference. The inset shows the spin density distribution (isosurface at 0.02 e^-/Å) within the cluster, which resides predominantly on two metal cores.*

The 3D spin density distribution in the inset of the Fig. 3 clearly indicates that the unpaired electrons are predominantly located at the Cr atoms of the encapsulated dimer. However, there are two protrusions of the spin density through two hexagonal facets of the cage, which indicate some spin density delocalization over the adjacent Si-Si bonds. Consistent with this explanation, the density of states (DOS) plot depicts that, despite the predominance of the Cr in the last peak in the occupied orbitals area (around -9 eV), which agrees nicely with the position of the ten unpaired *d*-electrons in the isolated Cr_2^+ dimer, there is a small fraction of cage Si atoms contributing to this peak.

The picture gets further support from the total density difference analysis (Fig. 4a). For this, we subtract the sum of the total densities of the empty $Si_{24}H_{24}$ cage and the isolated Cr_2^+ dimer from the total density of the $Cr_2^+@Si_{24}H_{24}$ aggregate. The resulting total density (blue regions indicate more electronic density, i.e. more negative charge) shows that in the $Cr_2^+@Si_{24}H_{24}$ aggregate there is more electronic density located at the edges of the structure (connecting Cr atoms with the hexagonal facets of the cage). At the same time the small red-colored areas at the Cr atoms indicate that there was slightly higher electron density on Cr atoms in the isolated dimer. This suggests that a fraction of the *d*-electrons, located at the Cr cores in the

isolated dimer, are now partially re-distributed in the area between the outer sides of the dimer and the hexagonal facets of the cage, however still located mostly at the metal core. On the other hand, the one remaining unpaired *s*-electron, through which binding in the isolated Cr_2^+ dimer was mediated, is intact, which is indicated by the zero total density difference between the Cr cores, and is also reflected by the conserved Cr-Cr equilibrium distance.

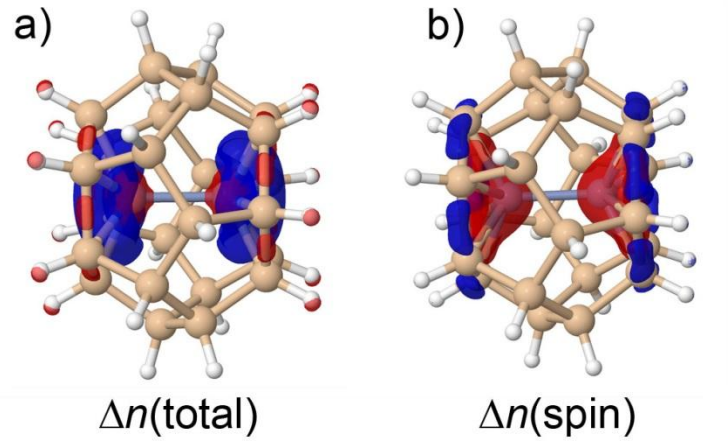

Fig. 4. *3D distribution of the (a) total electron density difference* $\Delta n=[n(Cr_2^+@Si_{24}H_{24}) - n(Si_{24}H_{24}) - n(Cr_2^+)]$ *and (b) spin density difference* $\Delta n=[n(Cr_2^+@Si_{24}H_{24}) - n(Cr_2^+)]$ *calculated at the hybrid PBE0 functional level; blue color depicts regions with more electron density. Note that here enlarged (0.015* e^-*/Å) isosurfaces are presented for clarity.*

This is in line with the spin density difference between the $Cr_2^+@Si_{24}H_{24}$ aggregate and the isolated Cr_2^+ dimer, depicted in Fig. 4b. Here one can see that in the resulting $Cr_2^+@Si_{24}H_{24}$ aggregate, there is more spin density located at the outskirts of the cluster (Si-Si bonds within the two hexagonal facets) and less spin density at the Cr cores, compared to the isolated Cr_2^+ dimer. However, the spin density between the cores stays the same, as indicated by the zero density difference in this area, and by the total spin density distribution within the cluster (inset in the Fig. 3). Thus one can conclude that, while the overall high spin state of the structure is conserved, the additional interaction via the adjacent hexagonal facets of the cage helps to stabilize the resulting aggregate, which is also reflected in the large HOMO-LUMO gap value of 2.74 eV.

We have also run global geometry optimization and subsequent electronic structure analysis of the identified ground-state structures for two other dopants (Mn_2^+, $CrMn^+$). Fig. 5 illustrates the obtained ground-state structures.

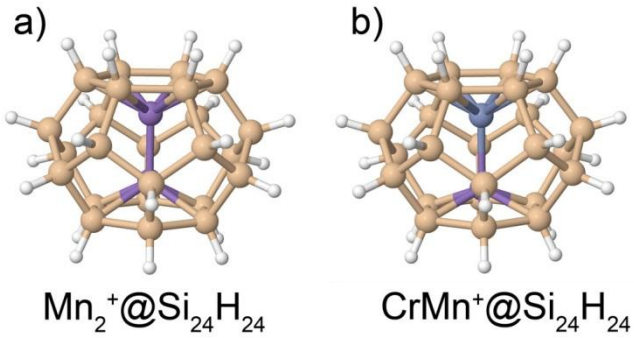

Fig. 5. *Ground-state structures of (a) $Mn_2^+@Si_{24}H_{24}$ (9 unpaired electrons, 2.59 Å Mn-Mn distance) and (b) $CrMn^+@Si_{24}H_{24}$ (10 unpaired electrons, 2.80 Å Cr-Mn distance).*

As expected, $CrMn^+$ encapsulated within the $Si_{24}H_{24}$ cage (see Fig. 5b) has an equilibrium distance close to the one observed for the isolated cluster (2.80 Å in both cases) and exhibits a high spin state of ten unpaired electrons.

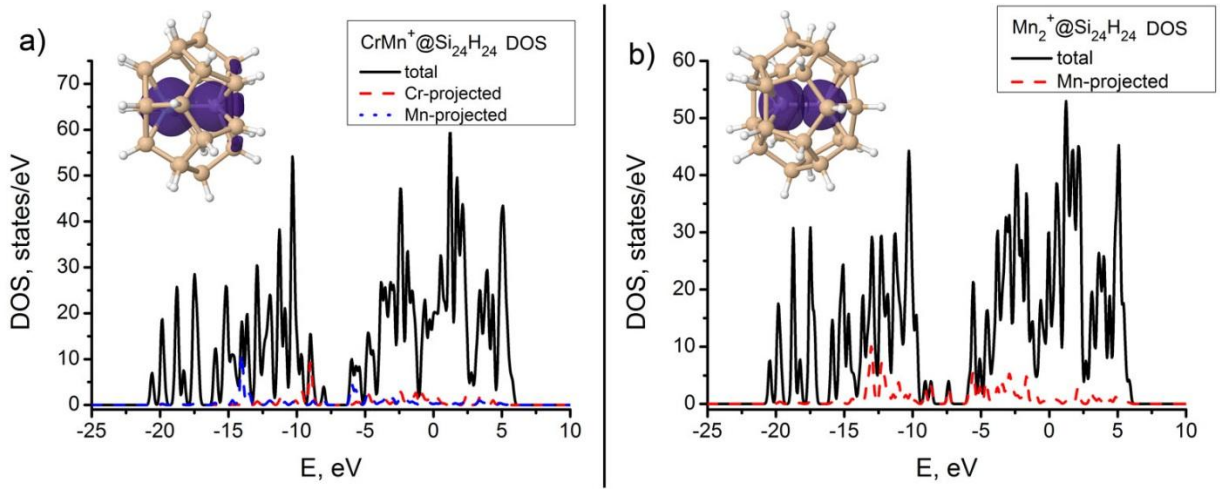

Fig. 6. *Total density of states and DOS projected on the metal dopants for (a) $CrMn^+@Si_{24}H_{24}$ (HOMO lies at -8.04 eV, LUMO at -6.02 eV) and (b) $Mn_2^+@Si_{24}H_{24}$ (HOMO lies at -7.38 eV, LUMO at -5.85 eV) aggregates.*

The analysis of the spin density distribution of $CrMn^+@Si_{24}H_{24}$ (see inset in Fig. 6a) reveals that the ten unpaired electrons are predominantly located at the metal cores, with the Mn atom (on the right in the inset picture) showing more interaction with the adjacent hexagonal facet of the Si cage. The density of states depicts two distinct peaks for the *d*-electrons located at the Cr and Mn cores, with their separate positions (near -9 eV and -13 eV, respectively, which

matches the positions of the corresponding electrons in the isolated $CrMn^+$ dimer reasonably well) suggesting a localized character of *d*-electrons belonging to Cr and Mn metal cores. Overall, it shows a very similar stabilization mechanism as was discussed for $Cr_2^+@Si_{24}H_{24}$ above, with some fraction of the Mn electrons partially delocalized over the adjacent hexagonal cage facet, and the Cr atom compensating for this by shifting some of its electronic density along the Cr-Mn bond towards Mn (see Fig.7a). The lower degree of interaction between the encapsulated dopant and the surrounding cage compared to the $Cr_2^+@Si_{24}H_{24}$ case (compare Fig. 6a and Fig. 3), is reflected in less delocalization of the spin density and sharper metal-projected DOS peaks. Besides, it is also supported by a smaller value of the binding energy (2.67 eV for $CrMn^+@Si_{24}H_{24}$ vs. 3.26 eV for $Cr_2^+@Si_{24}H_{24}$).

The $Mn_2^+@Si_{24}H_{24}$ aggregate shows slightly different behavior. Here also the unpaired electrons, as expected, are predominantly located at the two Mn metal cores (see inset in Fig. 6b). Two distinct peaks around -13 eV in the DOS plot support this view. However, the total number of unpaired electrons is not eleven as might be expected from the analogy with the $Cr_2^+@Si_{24}H_{24}$ results, but only nine. To figure out where this additional electron paring comes from, we take a look at the spin density difference between the $Mn_2^+@Si_{24}H_{24}$ aggregate and the Mn_2^+ dimer with nine unpaired electrons (Fig. 7b). Here the additional electron density between the metal cores (blue region) clearly indicates additional binding in the encapsulated dimer compared to the isolated one. This suggests that one additional *d*-electron can be used together with the three remaining *s*-electrons to additionally stabilize the bond within the encapsulated dimer. This is also reflected in the shortened Mn-Mn distance (2.59 Å in $Mn_2^+@Si_{24}H_{24}$ aggregate vs. 2.93 Å in Mn_2^+ dimer).

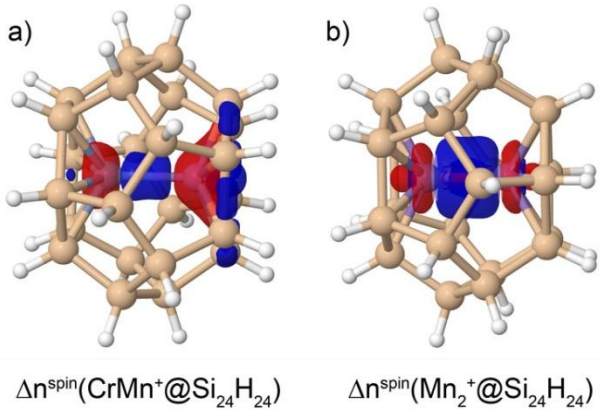

Fig. 7. *3D distribution of the spin density difference (a) $\Delta n=[n(CrMn^+@Si_{24}H_{24}) - n(CrMn^+)]$ and (b) $\Delta n=[n(Mn_2^+@Si_{24}H_{24}) - n(Mn_2^+, 10\text{-tet})]$*

Additionally, the $Mn_2^+@Si_{24}H_{24}$ structure exhibits the least interaction between the dopant and the cage among all three considered dopants (compare insets in Fig. 3 and Fig. 6), which is also reflected in the smallest binding energy value of 1.77 eV.

5. *References*

[1] V. Blum, R. Gehrke, F. Hanke, P. Havu, V. Havu, X. Ren, K. Reuter, M. Scheffler, "Ab initio Simulations with Numeric Atom-Centered Orbitals", *Comp. Phys. Comm.* **180**, 2175 (2009), http://dx.doi.org/10.1016/j.cpc.2009.06.022

[2] X. Ren, P. Rinke, V. Blum, J. Wieferink, A. Tkatchenko, A. Sanfilippo, K. Reuter, M. Scheffler, "Resolution-of-Identity Approach to Hartree-Fock, Hybrid Density Functionals, RPA, MP2 and GW with Numeric Atom-Centered Orbital Basis Functions", *New. J. Phys.* **14**, 053020 (2012), http://dx.doi.org/10.1088/1367-2630/14/5/053020

[3] C. Adamo, V. Barone, "Toward Reliable Density Functional Methods Without Adjustable Parameters: The PBE0 Model", *J. Chem. Phys.* **110**, 6158 (1999), http://dx.doi.org/10.1063/1.478522

[4] W. K. Press, S. A. Teukolsky, W. T. Vetterlin, B. T. Flannery, "Numerical Recipes: the Art of Scientific Computing", Cambridge University Press, Cambridge, 2007, http://www.worldcat.org/isbn/0-521-88068-8

[5] D. J. Wales, J. P. K. Doye, "Global Optimization by Basin-Hopping and the Lowest Energy Structures of Lennard-Jones Clusters Containing up to 110 Atoms", *J. Phys. Chem. A* **101**, 5111 (1997), http://dx.doi.org/10.1021/jp970984n

[6] D. J. Wales, J. P. K. Doye, M. A. Miller, P. N. Mortenson, T. R. Walsh, "Energy Landscapes: From Clusters to Biomolecules", *Adv. Chem. Phys.* **115**, 1 (2000), http://dx.doi.org/10.1002/9780470141748.ch1

[7] R. Gehrke, K. Reuter, "Assessing the efficiency of first-principles basin-hopping sampling", *Phys. Rev. B* **79**, 085412 (2009), http://dx.doi.org/10.1103/PhysRevB.79.085412

[8] N. Metropolis, A. W. Rosenbluth, M. N. Rosenbluth, A. H. Teller, E. Teller, "Equation of State Calculations by Fast Computing Machines", *J. Chem. Phys.* **21**, 1087 (1953), DOI: http://dx.doi.org/10.1063/1.1699114

[9] V. Kumar, Y. Kawazoe, "Hydrogenated Silicon Fullerenes: Effects of H on the Stability of Metal-Encapsulated Silicon Clusters", *Phys. Rev. Lett.* **90**, 055502 (2003), http://dx.doi.org/10.1103/PhysRevLett.90.055502

[10] W. Ji, C. Luo, "Structures, Magnetic Properties, and Electronic Counting Rule of Metals-Encapsulated Cage-like M_2Si_{18} (M = Ti-Zn) clusters", *Int. J. Quantum Chem.* **112**, 2525 (2012), http://dx.doi.org/10.1002/qua.23245

[11] H. Kawamura, V. Kumar, Y. Kawazoe, „Growth, magic behavior, and electronic and vibrational properties of Cr-doped Si clusters", *Phys. Rev. B* **70**, 245433 (2004), http://dx.doi.org/10.1103/PhysRevB.70.245433

[12] F. Hagelberg, C. Xiao, and W. A. Lester, Jr., "Cagelike Si_{12} clusters with endohedral Cu, Mo, and W metal atom impurities", *Phys. Rev. B* **67**, 035426 (2003), http://dx.doi.org/10.1103/PhysRevB.67.035426

[13] D. Palagin, M. Gramzow, K. Reuter, "On the stability of "non-magic" endohedrally doped Si clusters:A first-principles sampling study of MSi_{16}^+ (M = Ti,V,Cr)", *J. Chem. Phys.* **134**, 244705 (2011), http://dx.doi.org/10.1063/1.3604565

[14] K. A. Jackson, E. Kaxiras, M. R. Pederson, "Bonding of Endohedral Atoms in Small Carbon Fullerenes", *J. Phys. Chem.* **98**, 7805 (1994), http://dx.doi.org/10.1021/j100083a010

[15] M. B. Torres, E. M. Fernández, L. C. Balbás, "Theoretical Study of Isoelectronic Si_nM clusters (M = Sc^-, Ti, V^+; n = 14-18)", *Phys. Rev. B* **75**, 205425 (2007), http://dx.doi.org/10.1103/PhysRevB.75.205425

[16] D. Palagin, K. Reuter, "$MSi_{20}H_{20}$ Aggregates: From Simple Building Blocks to Highly Magnetic Functionalized Materials", *ACS Nano* **7**, 1763 (2013), http://dx.doi.org/10.1021/nn3058888

[17] D. Palagin, K. Reuter, "Evaluation of Endohedral Doping of Hydrogenated Si Fullerenes as a Route to Magnetic Si Building Blocks", *Phys. Rev. B* **86**, 045416 (2012), http://dx.doi.org/10.1103/PhysRevB.86.045416

[18] V. Kumar, Y. Kawazoe, "Hydrogenated Silicon Fullerenes: Effects of H on the Stability of Metal-Encapsulated Silicon Clusters", *Phys. Rev. Lett.* **90**, 055502 (2003), http://dx.doi.org/10.1103/PhysRevLett.90.055502

[19] V. Kumar, Y. Kawazoe, "Hydrogenated Caged Clusters of Si, Ge, and Sn and Their Endohedral Doping with Atoms: Ab initio Calculations", *Phys. Rev. B* **75**, 155425 (2007), http://dx.doi.org/10.1103/PhysRevB.75.155425

[20] M. S. Bahramy, V. Kumar, Y. Kawazoe, "First-Principles Calculations of Hyperfine Structure in M-doped $Si_{16}H_{16}$ Fullerene Cages (M = Cr, Mn, and Fe)", *Phys. Rev. B* **79**, 235443 (2009), http://dx.doi.org/10.1103/PhysRevB.79.235443

[21] J. T. Lau, K. Hirsch, A. Langenberg, J. Probst, R. Richter, J. Rittmann, M. Vogel, V. Zamudio-Bayer, T. Möller, B. von Issendorff, "Localized High Spin States in Transition-Metal Dimers: X-ray Absorption Spectroscopy Study", *Phys. Rev. B* **79**, 241102 (2009), http://dx.doi.org/10.1103/PhysRevB.79.241102

[22] G. Frenking, I. Antes, M. Böhme, S. Dapprich, A.W. Ehlers, V. Jonas, A. Neuhaus, M. Otto, R. Stegmann, A. Veldkamp, S. F. Vyboishchikov, "Pseudopotential Calculations of Transition Metal Compounds: Scope and Limitations", Rev. Comp. Chem. 8, 63 (1996), http://dx.doi.org/10.1002/9780470125854.ch2

[23] T. R. Cundari, M. T. Benson, M. L. Lutz, S. O. Sommerer, "Effective Core Potential Approaches to the Chemistry of the Heavier Elements", Rev. Comp. Chem. 8, 145 (1996), http://dx.doi.org/10.1002/9780470125854.ch3

[24] C. S. Garoufalis, A. D. Zdetsis, S. Grimme, "High Level Ab Initio Calculations of the Optical Gap of Small Silicon Quantum Dots", Phys. Rev. Lett. 87, 276402 (2001), http://dx.doi.org/10.1103/PhysRevLett.87.276402

[25] C. J. Cramer, D. G. Truhlar, "Density Functional Theory for Transition Metals and Transition Metal Chemistry", *Phys. Chem. Chem. Phys.* **11**, 10757 (2009), http://dx.doi.org/10.1039/b907148b

[26] C.-X. Su, D. A. Hales, P. B. Armentrout, "The Bond Energies of Cr_2 and Cr_2^+", *Chem. Phys. Lett.* **201**, 199 (1993), http://dx.doi.org/10.1016/0009-2614(93)85056-T

[27] M. F. Jarrold , A. J. Illies , M. T. Bowers, "Photodissociation of the Dimanganese Ion: Mn_2^+: a Route to the Energetics of Metal Clusters", *J. Am. Chem. Soc.* **107**, 7339 (1985), http://dx.doi.org/10.1021/ja00311a021

[28] V. E. Bondybey, J. H. English, "Electronic Structure and Vibrational Frequency of Cr_2", *Chem. Phys. Lett.* **94**, 443 (1983), http://dx.doi.org/10.1016/0009-2614(83)85029-5

[29] B. Simard, M.-A. Lebeault-Dorget, A. Marijnissen, J. J. ter Meulen, "Photoionization Spectroscopy of Dichromium and Dimolybdenum: Ionization Potentials and Bond Energies", *J. Chem. Phys.* **108**, 9668 (1998), http://dx.doi.org/10.1063/1.476442

[30] M. Cheeseman, R. J. Van Zee, H. L. Flanagan, W. Weltner, "Transition-Metal Diatomics: Mn_2, Mn_2^+, CrMn", *J. Chem. Phys.* **92**, 1553 (1990), http://dx.doi.org/10.1063/1.458086